ISBN: 978-628-95207-4-3. ISSN: 2414-6390. Digital Object Identifier: https://dx.doi.org/10.18687/LACCEI2023.1.1.1595

Improving the resolution of STED microscopy using the SUPPOSe algorithm

Micaela Toscani, PhD[1*], and Axel M. Lacapmesure, PhD candidate[2**]
[1]*Consejo Nacional de Investigaciones Científicas y Técnicas (CONICET), Buenos Aires, Argentina.*
[2]*Laboratorio de Fotónica, Instituto de Ingeniería Biomédica, Facultad de Ingeniería UBA, Buenos Aires, Argentina*
*mtoscani@fi.uba.ar , **alacapmesure@fi.uba.ar

Abstract*– Here we apply the gSUPPOSe algorithm on images acquired using Stimulated Emission Depletion (STED) microscopy with the aim of improving the resolution limit achieved. We processed images of the nuclear pore complex (NPC) from cell lines in which the Nup96 nucleoporin was endogenously labeled. This reference protein forms a ring whose diameter is ~107 nm with 8 corners ~42 nm apart from each other. The stereotypic arrangement of proteins in the NPC has been used as reference structures to characterize the performance of a variety of microscopy techniques. STED microscopy images resolve the ring arrangement but not the eightfold symmetry of the NPC. After applying the gSUPPOSe algorithm to the STED images, we were able to solve the octagonal structure of the NPC. After processing 500 Regions Of Interest (ROIs), the average radius of the NPC was found to be R = 54.2 ± 2.9 nm, being consistent with the theoretical distances of this structure. To verify that the solutions obtained are compatible with a NPC-type geometry, we rotate the solutions to optimally fit an eightfold-symmetric pattern and we count the number of corners that contain at least one localization. Fitting a probabilistic model to the histogram of the number of bright corners gives an effective labeling efficiency (ELE) of 31%, which is in agreement with the values reported in for other cell lines and ligands used in STORM images, showing that SUPPOSe can reliably retrieve sub-resolution, nanoscale objects even in such noisy conditions.

***Keywords--** Microscopy, STED, SUPPOSe, NPC, Superresolution.*

I. Introduction

In fluorescence microscopy, each acquired sample is the result of a noise process acting on the convolution between an underlying object —an arrangement of fluorescent proteins tied to the things we want to see— with the microscope response function —known as Point Spread Function or PSF. SUPPOSe is a convolution-based algorithm for improving microscopy images that relies on representing the object under microscope as a SUPperposition of POint SourcEs with the same intensity [1-8]. By knowing the instrument Point-Spread Function (PSF) and the image formation model, the optimum position of these sources can be retrieved by iteratively solving an optimization problem that results in a description of the object with better resolution than the image itself. The best source positions are retrieved after running gSUPPOSe, a gradient-based iterative solver for the SUPPOSe optimization problem [5-6]. The inputs of the algorithm are: the sample, the PSF and an initial solution as an array of 2D vectors. The program returns the best fitted positions and intensity. A reconstruction image may be obtained afterwards by convolving with a smaller PSF, where sub-resolution properties of the original object may be recovered. A schematic diagram of the operation of the gSUPPOSe algorithm is shown in Fig 1. The code of gSUPPOSe is freely available at the public repository https://gitlab.com/labofotonica/gsuppose [6].

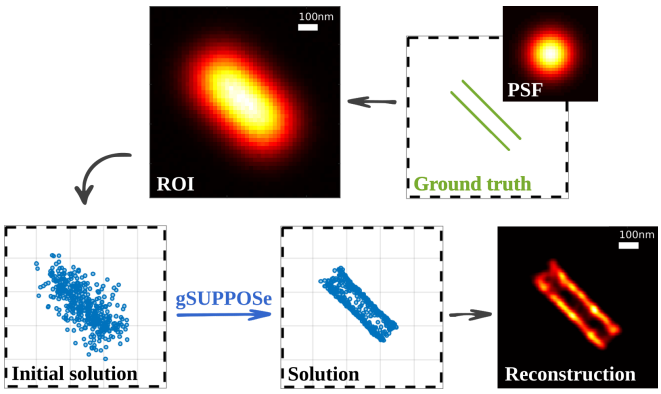

Fig. 1 Schematic diagram of how SUPPOSe solutions are obtained. A random distribution of virtual sources is proposed as the initial solution, from where gSUPPOSe fits the best positions, recovering sub-resolution features.

Here we apply SUPPOSe to Stimulated Emission Depletion (STED) microscopy, a super-resolution technique based on experimentally shaping the PSF by exploiting the photophysics of fluorophore activation. We analyze images of the human Nuclear Pore Complex (NPC, a known nanometric structure well suited for microscopy assessment) and compare our results with other localization-based super-resolution methods, like STORM.

II. Method

The SUPPOSe algorithm can be applied to any microscopy technique where the acquired image S can be modeled as a convolution between the ground truth structure and the point spread function of the optical system,

Digital Object Identifier: (only for full papers, inserted by LACCEI).
ISSN, ISBN: (to be inserted by LACCEI).
DO NOT REMOVE

$$S(r) = \mathcal{N}[R(r) * PSF(r)] \quad (1)$$

where S is the acquired image, R is the unknown underlying ground truth structure, PSF is the point spread function of the imaging system and $\mathcal{N}(\cdot)$ is a noise process. In this case $r \in \mathbb{R}^2$ represents the coordinate in which the measurement is carried out. The image deconvolution problem is mathematically ill posed. Due to the measurement noise, a direct inversion of the problem leads to results without physical meaning. The SUPPOSe algorithm converts the problem of finding the intensity of the source as a function of position into that of finding positions of virtual sources of equal intensity in order to reconstruct the acquired image. If we want to reconstruct information with different intensities, we simply accumulate a greater or lesser number of virtual sources in that area.

The SUPPOSe algorithm assumes that the function R (for example, the distribution of fluorophores in a fluorescent sample) can be modeled as a superposition of M point sources of equal intensity α (called virtual sources),

$$R(r) \sim \alpha \sum_{k=1}^{M} \delta(r - p_k) \quad (2)$$

where $p_k \in \mathbb{R}^2$ $(k = 1 \dots M)$ are the positions of the virtual sources and δ is the Dirac delta function. Note that these virtual sources lie in the continuous space and are not restricted to a pixel grid. By taking the convolution product with the PSF, we obtain a reconstructed, noiseless image C,

$$C(r) = \alpha \sum_{k=1}^{M} PSF(r - p_k), \quad (3)$$

that approximates the sample that would be acquired. SUPPOSe works by finding the set of positions p_k which minimizes some fitness function $F(S, C)$ that measures the similarity between the sample S and the reconstruction C. In this case we find a local optimum for the p_k positions by performing an iterative search based on gradient calculation [9]. To perform the optimization, we take the fitness F (over all pixels $i = 1 \dots N_{px}$) as the mean squared error,

$$F(S, C) = \frac{1}{N_{px}} \sum_{i=1}^{N_{px}} (s_i - c_i)^2. \quad (4)$$

Gradient descent methods are based on updating the parameters (i.e. the positions p_k of the virtual sources) in some direction determined by gradient $\nabla_{p_k} F$ by some amount controlled by a parameter η called the learning rate. The most straightforward update rule for a gradient descent method for SUPPOSe is to simply move the source positions in the opposite direction of the gradient (since we want to minimize F). Therefore the positions at iteration t are given by

$$p_k(t) = p_k(t - 1) - \eta \nabla_{p_k} F \quad (5)$$

In stochastic gradient descent optimization, instead of applying the update rule to all the positions at once, first the positions are randomly splitted in batches of a fixed size and then the update rule is applied to each batch separately. By controlling the batch size one can balance the computational load (since C and the gradients are calculated once per batch) against how finely grained the solution space is explored (which improves convergence). By combining stochastic optimization with a more sophisticated update rule that follows the Adaptive Moment estimation (ADAM) algorithm, a universal, adaptive optimization algorithm with low number of free parameters is obtained [10-13].

It has been shown that the SUPPOSe algorithm, under normal measurement noise conditions, recovers the object with a resolution more than three times better than that provided by the instrument. In this work it is shown that combining SUPPOSe with another superresolution microscopy technique can further extend the resolution limit obtained.

We processed with gSUPPOSe images of the human nuclear pore complex acquired with the STED microscopy technique. STED microscopy is a type of super-resolution microscopy technique that can bypass the diffraction limit of light microscopy to increase resolution [14]. STED exploits the nonlinear response of fluorophores used to label biological samples. The fluorescence process occurs by exciting an electron from the ground state to an excited electronic state of a different energy level which, after relaxing back to the ground state, emits a photon at the corresponding emission wavelength. STED interrupts this process before the photon is released and forces the excited electron to relax into a higher vibrational state than it would enter in the fluorescence transition, causing the released photon and its wavelength to be shifted farther into the red end of the spectrum. This shift differentiates the two types of photons, and allows the stimulated photon to be ignored. To achieve this, STED uses two laser excitation beams, one to achieve the fluorescence phenomenon and the other in the form of a donut to achieve fluorescence depletion in the donut area. In this way the STED technique has an effective PSF much narrower than that determined by the diffraction limit of light.

In this work, STED images of cell lines were used in which the Nup96 nucleoporin present in the NPC structure was endogenously labeled [15]. This reference protein forms a ring whose diameter is ~107 nm with 8 corners ~42 nm apart from each other [16]. The stereotypic arrangement of proteins in the NPC has been used as reference structures to characterize the performance of a variety of microscopy techniques. The images of the samples were acquired in an Abberior STED/RESOLFT microscope and the pixel size corresponds to 15 nm in the sample. The STED images were

acquired by donut-shaped depletion using a 775 nm pulsed laser along with a 640 nm pulsed laser exciting STAR 635P tagged Nup96-mEGFP. Emission was collected using a 685/70 nm bandpass filter. A region of the image is shown in Fig. 2b. The raw images used are available in the public repository BioStudies www.ebi.ac.uk/biostudies/studies/S-BSST257.

Usually the PSF is obtained empirically by imaging sub-resolved structures under the same system conditions (optics and specimen environment) used to image the sample. In the case of STED microscopy it is important to estimate the PSF directly from the image being deconvolved since the PSF is strongly dependent on the photophysics of the fluorescent marker [17-20]. The common approach of using fluorescent beads can result in an wrong estimate of the PSF, since in most cases the fluorescent label used for the beads is different from that used to label the sample.

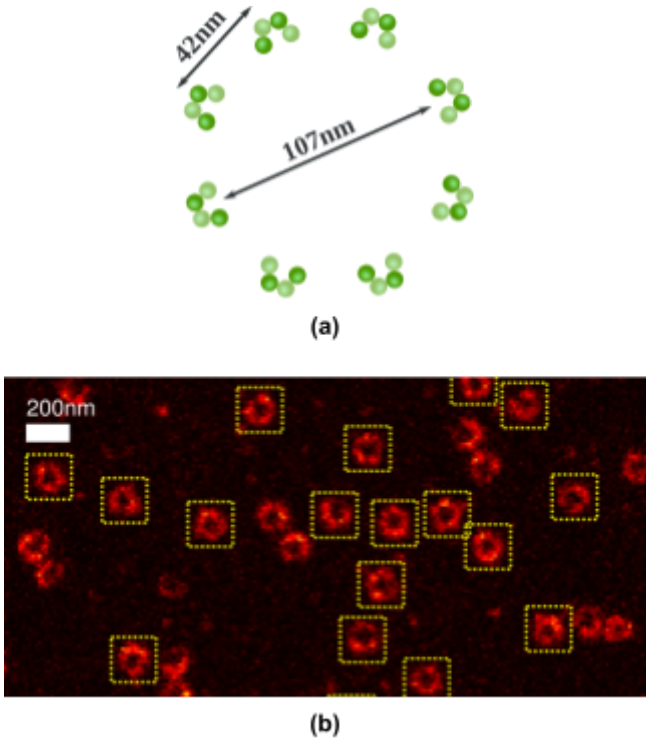

Fig. 2 The nuclear pore complex (NPC) structure. (a) Top view schematic and characteristic distances. (b) Raw STED image of Nup96-GFP labeled with an AberriorStar635P-coupled anti-GFP nanobody.

We used the Nup-96 proteins as a sub-resolved point-like source to estimate the PSF function from the same STED image. We took multiple radial profiles of the NPC rings in the STED images and we fit a Gaussian PSF with a size of σ ~ 20 nm.

$$PSF(r) = A\,exp(-\frac{r^2}{2\sigma^2}) \qquad (6)$$

When observing the NPCs by widefield microscopy, they are observed as diffuse spots without structure information. STED microscopy images resolve the ring-like arrangement but not the eightfold symmetry of the NPC. After applying the gSUPPOSe algorithm to the STED images, we were able to solve the octagonal structure of the NPC as can be seen in Fig. 3b.

In gSUPPOSe, most of the computational time is spent evaluating the convolutions of the virtual sources with the PSF and its derivatives. Since the positions p_k lie in continuous space and we want to keep PSF as arbitrary as possible, the usual speed-optimized routines (as the methods based in Discrete Fourier Transform) do not apply. Instead we have developed an auxiliary library, namely CaTMU, to calculate all the convolutions of SUPPOSe in a time and resource efficient way. CaTMU is written in C++ and CUDA, including a Python API [21].

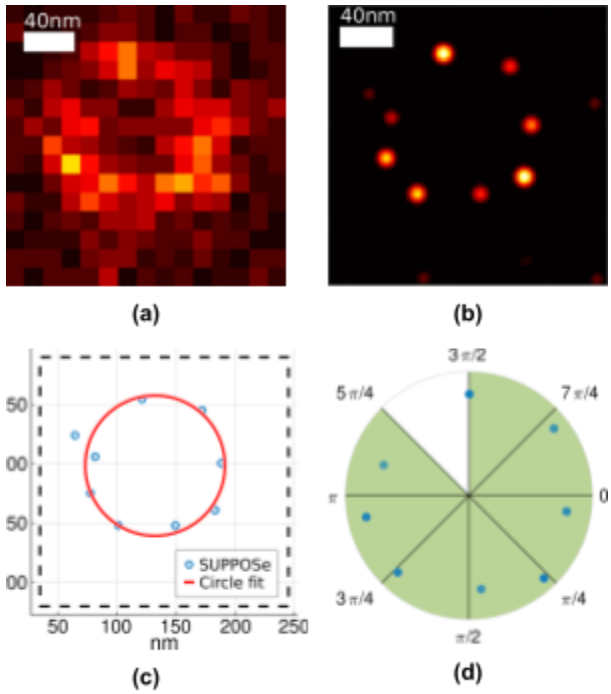

Fig. 3 Results of SUPPOSe on a single STED image. (a) Region of interest processed with the algorithm, (b) SUPPOSe reconstruction, (c) the radius of the structure was determined by fitting the SUPPOSe coordinates (algorithm output) with a circular model, (d) the solution was rotated to optimally fit an eightfold-symmetric template and and the corners containing at least one location were counted.

III. Results

We processed with gSUPPOSe 500 regions of interest (ROIs) corresponding to NPC structures in the sample. In all cases, the reconstructions obtained were able to distinguish an underlying structure within the NPC ring detected in the STED images. We quantify the quality of the reconstructions using some metrics proposed in [15] and compare the results with those obtained after processing this same sample with

single molecule localization techniques, such as STORM or PALM [22,23].

The first analysis we performed was to estimate the radius of the NPC reconstructions obtained. We first rule out from the SUPPOSE solutions the isolated virtual sources, those that have no nearest neighbors within a 0.1px radius around them. Then the radius of the circular NPC structures was determined by directly fitting the coordinates of the virtual sources with a circular model treating the position of the center and the radius as free fitting parameters, as seen in Fig. 3c. The histogram of fitted radius for all SUPPOSe solutions is shown in Fig. 4. After processing 500 ROIs, the average radius of the NPC was found to be R = 54.2 ± 2.9 nm, being consistent with the theoretical distances of this structure.

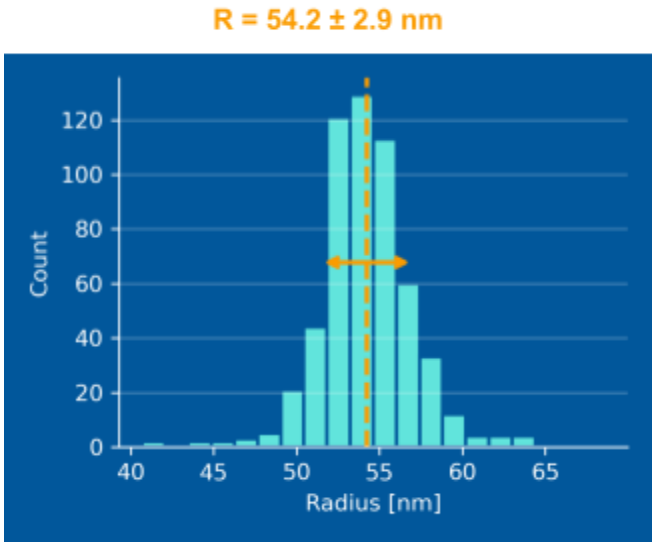

Fig. 4 Histogram of fitted radius for all NPC images. The orange line and arrow indicates mean and standard deviation of R = 54.2 ± 2.9 nm.

Another analysis we perform is to evaluate if the structure reconstructed by SUPPOSe matches the octagonal geometry of the NPC. In this line, it must be taken into account that the SUPPOSe solution could depend on how densely the NPC structures are decorated with fluorophores. This can be described by the Effective Labeling Efficiency (ELE), which represents the fraction of target proteins carrying a fluorophore that achieves to be detected by the observing optical system. When the ELE is low, NPCs appear as incomplete rings with missing corners. To quantify the ELE we counted the number of corners detected in each SUPPOSe solution. The positions of the virtual sources were converted into polar coordinates (r_i, φ_i) and we discard virtual sources that are too close to the center of the ring or too far away ($30\,nm < r_i < 70\,nm$). We find the rotation of the structure by minimizing

$$\varphi_{rot} = arg\,min(\varphi_{rot} - \varphi_i \, mod \, \tfrac{\pi}{4}). \qquad (9)$$

We rotate the SUPPOSe solutions to optimally fit the eightfold symmetric template and count the number of slices that contain at least one detected corner within, as seen in Fig. 3d. The histogram of the number of corners detected for all SUPPOSe solutions is shown in Fig. 5.

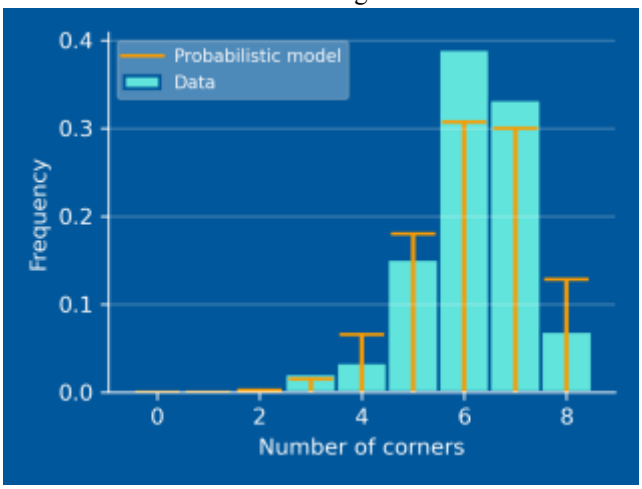

Fig. 5 Histogram of number of bright corners per NPC along with the predicted values from the fitted probabilistic model, giving an effective label efficiency ELE = 31%.

The effective labeling efficiency can be modeled using the binomial probability distribution. The binomial probability density function

$$B(k|n,p) = \binom{n}{k} p^k (1-p)^{n-k} \qquad (10)$$

describes the probability of getting k successes in n independent Bernoulli trials, where the successes occur with probability p and the failures occur with probability $(1-p)$. When looking at the structure of the NPC from above, each corner has 4 proteins as schematized in Fig. 2, and each protein has a probability p_{label} of being tagged. Thus, the probability of a corner of the NPC to be dark becomes $p_{dark} = B(0|4, p_{label})$, and the probability to see a corner with at least one label is $p_{bright} = 1 - p_{dark}$. In this way we can model the probability of N out of 8 corners being visible as

$$p(N|p_{label}) = B(N|8, p_{bright})$$
$$p(N|p_{label}) = B(N|8, 1 - B(0|4, p_{label})) \qquad (11)$$

Fitting a probabilistic model to the histogram of the number of bright corners (Fig. 5) gives an effective labeling efficiency (ELE) of 31%, which is in agreement with the values reported in for other cell lines and ligands used in STORM images [15].

Another analysis performed was the impact on the SUPPOSe solution of potential uncertainties in the PSF measurement, due to the intrinsic conditioning of measuring

the PSF of STED mentioned above. For this reason, we process the same ROI of the sample by varying the size of the PSF used to process with respect to the PSF measured experimentally. In Fig. 6 some results are shown after varying the width of the PSF by ± 30% with respect to the measured PSF. We observe the expected behavior for the SUPPOse algorithm under these conditions, when we process with a narrower PSF the algorithm starts having convergence problems and it becomes more difficult to define certain regions of the structure. This looks like a more diffuse

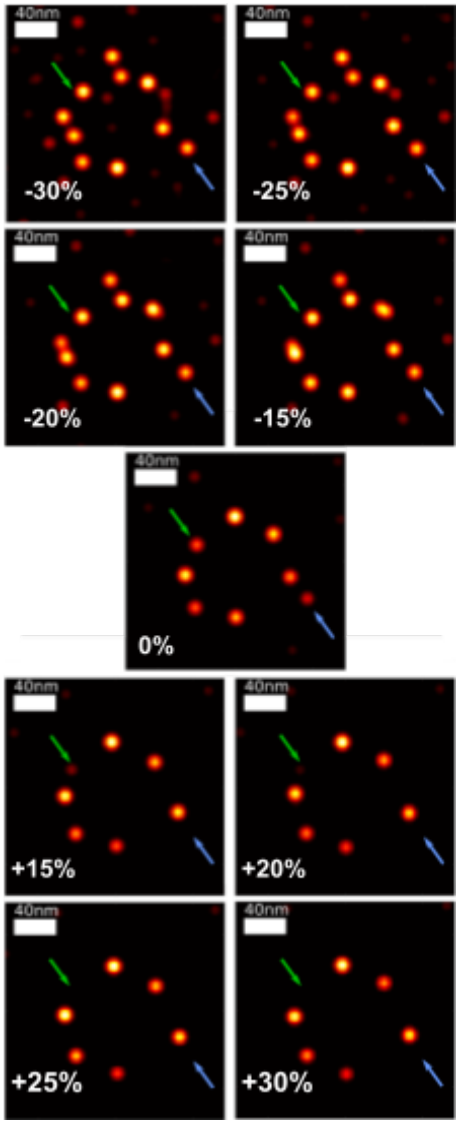

Fig. 6 SUPPOSe reconstructions for the same sample but varying the processing PSF size with respect to the measured experimental PSF in a range of ±30%.

distribution of virtual sources, which in certain places fails to define structure. In the opposite way, when we use a larger PSF the algorithm tends to overfit the information present in the image, tending to overcrowd the virtual sources. Despite these differences, it should be noted that the SUPPOSe algorithm can find the underlying structure in the image and reveal the information that is masked in the STED image. In Fig. 7 it can be seen that in a range within ± 10% of the size of the PSF used, the differences between the SUPPOSe solutions are negligible.

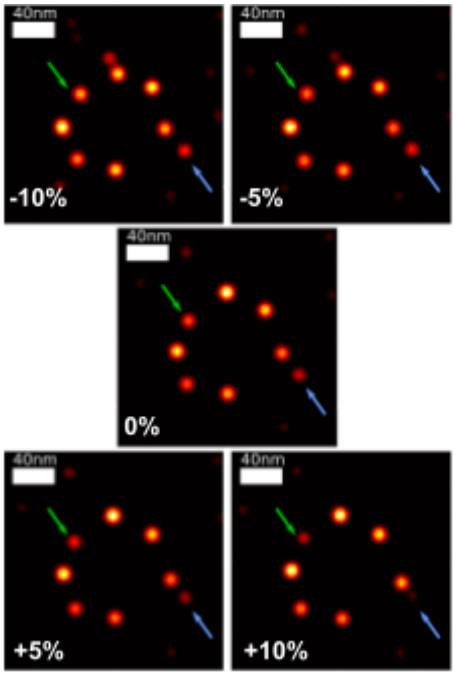

Fig. 7 SUPPOSe reconstructions for the same sample but varying the processing PSF size with respect to the measured experimental PSF in a range of ±10%.

IV. Conclusions

The SUPPOSe algorithm can process STED images to enhance the description of the underlying object. Description of human NPC nanostructures from SUPPOSe solutions is accurate and in agreement with expected shapes and label photophysics. SUPPOSe solutions can provide the same information as methods with better resolution than STED (like some Single Localization Microscopies). Experimental variations in the PSF do not significantly affect the algorithm.

Funding

Agencia Nacional de Promoción Científica y Tecnológica (BID PICT-2020- SERIEA-00617). Consejo Nacional de Investigaciones Científicas y Técnicas, CONICET (PIP 1184).

References

[1] Sandra Martínez, Micaela Toscani, Oscar E. Martínez Super-resolution method for a single wide field image deconvolution by superposition of point sources. J. Microscopy. May 2019, 275(1), pp. 51–65 https://doi.org/10.1111/jmi.12802.

[2] Micaela Toscani, Sandra Martínez, Oscar E. Martínez, "Single image deconvolution with super-resolution using the SUPPOSe algorithm," Proc. SPIE 10884, Single Molecule Spectroscopy and Superresolution Imaging XII, 1088415 (22 February 2019); doi: 10.1117/12.2508869
[3] Lacapmesure, A.M., Martínez, S., Martínez, O.E. "A new objective function for super-resolution deconvolution of microscopy images by means of a genetic algorithm", GECCO 2020 Companion - Proceedings of the 2020 Genetic and Evolutionary Computation Conference Companion, 2020, pp. 271–272
[4] M. Toscani, A. Mazzeo, S. Martínez, O. Martínez, A. Lacapmesure and G. B. Vazquez, "Fuentes de error, artificios, aceleración y validación del algoritmo de deconvolución con super-resolución para imágenes de microscopía," 2020 IEEE Congreso Bienal de Argentina (ARGENCON), 2020, pp. 1-7, doi: 10.1109/ARGENCON49523.2020.9505479.
[5] Axel M. Lacapmesure, Guillermo D. Brinatti Vazquez, Alejandro Mazzeo, Sandra Martínez, and Oscar E. Martínez, "Combining deep learning with SUPPOSe and compressed sensing for SNR-enhanced localization of overlapping emitters," Appl. Opt. 61, D39-D49 (2022).
[6] A. M. Lacapmesure, "gSUPPOSe repository," GitHub (2021) https://gitlab.com/labofotonica/ gsuppose [retrieved 5 January 2022].
[7] M. Toscani, S. Martinez, "Solving the boundary artifact for the enhanced deconvolution algorithm SUPPOSe applied to fluorescence microscopy", Computer Optics, 45:3 (2021), 418–426. DOI: https://doi.org/10.18287/2412-6179-CO-825
[8] Toscani, M., Martínez, O.E., Martínez, S "Resolution, accuracy and precision in super-resolved microscopy images using SUPPOSe" . Optics and Lasers in Engineering, 2023, 161, 107337.10.1117/12.2508904.
[9] Ruder, Sebastian. "An overview of gradient descent optimization algorithms." *arXiv preprint arXiv:1609.04747* (2016).
[10] Kingma, Diederik P., and Jimmy Ba. "Adam: A method for stochastic optimization." *arXiv preprint arXiv:1412.6980* (2014).
[11] Reddi, Sashank J., Satyen Kale, and Sanjiv Kumar. "On the convergence of adam and beyond." *arXiv preprint arXiv:1904.09237* (2019).
[12] Luo, Liangchen, et al. "Adaptive gradient methods with dynamic bound of learning rate." *arXiv preprint arXiv:1902.09843* (2019).
[13] T. Dozat, "Incorporating Nesterov momentum into ADAM," in Proceedings of 4th International. Conference on Learning Representations, Workshop Track, (2016).
[14] Hell, Stefan W., and Jan Wichmann. "Breaking the diffraction resolution limit by stimulated emission: stimulated-emission-depletion fluorescence microscopy." *Optics letters* 19.11 (1994): 780-782.
[15] Thevathasan, Jervis Vermal, et al. "Nuclear pores as versatile reference standards for quantitative superresolution microscopy." *Nature methods* 16.10 (2019): 1045-1053.
[16] Von Appen, Alexander, et al. "In situ structural analysis of the human nuclear pore complex." *Nature* 526.7571 (2015): 140-143.
[17] Zanella, Riccardo, et al. "Towards real-time image deconvolution: application to confocal and STED microscopy." *Scientific reports* 3.1 (2013): 2523.
[18] Westphal, Volker, and Stefan W. Hell. "Nanoscale resolution in the focal plane of an optical microscope." *Physical review letters* 94.14 (2005): 143903.
[19] Dyba, M., J. Keller, and S. W. Hell. "Phase filter enhanced STED-4Pi fluorescence microscopy: theory and experiment." *New journal of Physics* 7.1 (2005): 134.
[20] Dedecker, Peter, et al. "Orientational effects in the excitation and de-excitation of single molecules interacting with donut-mode laser beams." *Optics Express* 15.6 (2007): 3372-3383.
[21] A. Mazzeo, "CaTMU repository," GitHub (2021) https://github.com/alemazzeo/catmu [retrieved 5 January 2022].
[22] Betzig, Eric, et al. "Imaging intracellular fluorescent proteins at nanometer resolution." *science* 313.5793 (2006): 1642-1645.
[23] Rust, Michael J., Mark Bates, and Xiaowei Zhuang. "Stochastic optical reconstruction microscopy (STORM) provides sub-diffraction-limit image resolution." *Nature methods* 3.10 (2006): 793.